Light-ion-induced K-shell ionization in the adiabatic region

Ž. Šmit
J. Stefan Institute, University of Ljubljana, Ljubljana, Slovenia
(Received 27 January 1992)

K-shell ionization induced by fast ions was simulated by the excitation of a harmonic oscillator perturbed by time-dependent coupling of a parallel spring. Permanent coupling of the spring corresponds to the atom where both nuclei are united. In this adiabatic limit the two systems have an increased energy and reduced length scale. The ratio of the united-atom cross sections to the experimental ones was compared to the ratio of the oscillator excitation probabilities calculated in the adiabatic limit and by the coupled-channel method. Strong similiarities between the behavior of both types of ratios were observed, and it was pointed out that the adiabatic approximation overestimates the transition probabilities even at moderate collision velocities. The effective nuclear charges were deduced from the model and used for the cross-section calculation with hydrogenic Dirac wave functions. For the proton data, calculated and experimental cross sections agree within 10%. Due to the strong coupling of states in the adiabatic region, the effective nuclear charges exceed the united-atom limit by 20%.

PACS number(s): 34.10.+x, 34.50.Fa

I. INTRODUCTION

K-shell ionization induced by an adiabatic collision with an ion has been extensively treated within first-order perturbation theory, including higher-order effects as corrections [1]. In semiclassical calculations [2–4] using hyperbolic projectile trajectories and hydrogenic Dirac wave functions, the corrections are limited to the change of the electronic wave functions and binding energies due to the presence of the projectile charge. The traditional methods include the modification of the binding energy by the monopole term [5–7], the modification both of the binding energy and the effective nuclear charge [8–10], and the introduction of the polarized bound-state wave functions [11,12]. It is common to the methods [8–12] that for very slow collisions, the effective nuclear charge is given in the united-atom limit [8], i.e., by the sum of the projectile and the target atomic number corrected for the Slater screening constant. The united-atom nuclear charge and binding energy may even be used for fast collisions [8] and yield good values for the cross sections [4]. In order to study the united-atom approximation more thoroughly, we have repeated the proton-induced cross-section calculation [4] for some other target elements, and normalized the results to the averaged experimental data [13]. In Fig. 1, the cross-section ratio is shown with respect to the reduced projectile velocity ξ, defined by $\xi = 1/a_K q_0$ where a_K and $\hbar q_0$ are the K-shell radius and the minimum momentum transfer for adiabatic collisions, respectively. In general, the united-atom cross sections for $Z_2 \lesssim 50$ targets are underestimated for faster collisions, but largely exceed the experimental values for very slow collisions.

In the present study we would like to show that the difference between the united-atom cross section and the experimental one is mostly due to the coupling of states in the adiabatic region and therefore cannot be explained by the first-order approach. We shall replace the ion-atom collision system by a similar though simpler model which can be easily approached by the coupled-channel method. We propose to describe the K-shell ionization by an ion impact as the excitation of a harmonic oscillator perturbed by time-dependent coupling of an additional spring (Fig. 2). In the adiabatic limit, the atom and the oscillator respond in a similar way:

(i) The presence of an additional charge Z_1 in the vicinity of the nucleus Z_2 increases the atomic energy $(Z_2 - 0.3)^2$ Ry to $(Z_2 + Z_1 - 0.3)^2$ Ry. Parallel coupling

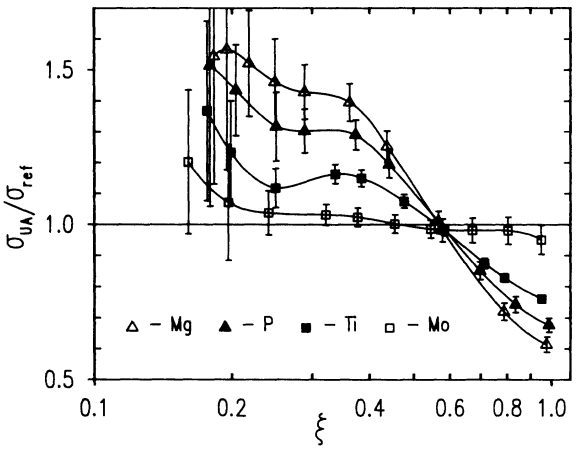

FIG. 1. The ratio between the semiclassical [4] and averaged experimental cross sections [13] as a function of the reduced projectile velocity ξ. The calculation used hydrogenic Dirac wave functions in the united-atom limit and included s and p partial waves. The solid lines were obtained by interpolation. The ratio Z_1/Z_2 varies approximately from 0.025 to 0.1.

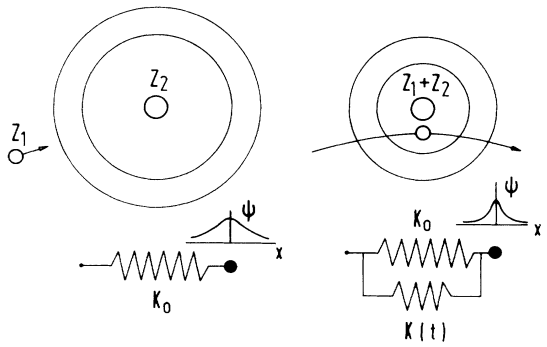

FIG. 2. Passage of an ion through the electron cloud corresponds to the time-dependent coupling of an additional spring to the harmonic oscillator.

of the spring with the constant K to the main spring K_0 increases the oscillator energy $\hbar\omega_0 = \hbar\sqrt{K_0/m}$ to $\hbar\omega = \hbar\sqrt{(K_0+K)/m}$.

(ii) The charge Z_1 reduces the K-shell radius $a_K = a_B/(Z_2 - 0.3)$ to $a_B/(Z_2 + Z_1 - 0.3)$. The length scale of the oscillator is given by $\sqrt{\hbar/m\omega}$ and has the same energy dependence as the K-shell radius in the atom. Coupling of the spring K results in a reduction of the oscillator wave function by a factor of $\sqrt[4]{1+K/K_0}$. For equivalence between both systems, the energy or length scale should change by the same factor. This implies for the spring constant K the relation

$$\left(1+\frac{Z_1}{Z_2-0.3}\right)^2 = \sqrt{1+\frac{K}{K_0}} \quad . \tag{1}$$

In the adiabatic limit, the excitation probability of the oscillator is calculated for the spring constant $K_0 + K$. The ratio between this and the exact excitation probability should thus be closely related to the ratio of the united-atom and experimental cross sections.

II. THEORY

A. The harmonic-oscillator model

Transitions in the harmonic oscillator are provoked by the perturbing potential $\frac{1}{2}Kx^2 f(t/\tau)$. The function f describes the time-dependent switching of the spring K with the characteristic time τ. The function f is maximal for $t = 0$ and approaches zero for $|t| \gg \tau$.

We shall expand the oscillator wave functions in the complete, orthonormal set of eigenstates of the unperturbed oscillator:

$$\Psi(x,t) = \sum_n a_n(t)\,\varphi_n(x)\,e^{-i(n+\frac{1}{2})\omega_0 t} \quad . \tag{2}$$

Since the oscillator is initially in its ground state, the initial values of a_n are

$$a_0(-\infty) = 1 \ , \qquad a_{n>0}(-\infty) = 0 \quad . \tag{3}$$

The set of coupled equations reads as

$$\dot{a}_f = -\frac{iK}{2\hbar}\sum_n a_n(t)\,\langle\varphi_f|x^2|\varphi_n\rangle\, f\left(\frac{t}{\tau}\right) e^{i(f-n)\omega_0 t} \quad . \tag{4}$$

It is convenient to rewrite (4) into a dimensionless form. So we define

$$\frac{K}{2m\omega_0^2} = v \ , \qquad \omega_0\tau = \lambda \ , \qquad \frac{t}{\tau} = s \ , \tag{5}$$

$$\langle\varphi_f|x^2|\varphi_n\rangle = \frac{\hbar}{m\omega_0}\langle x_{nf}^2\rangle \quad .$$

With the new quantities (5), Eq. (4) transforms into

$$\frac{da_f}{ds} = -iv\lambda\sum_n a_n(t)\,\langle x_{nf}^2\rangle\, f(s)\, e^{i(f-n)\lambda s} \quad . \tag{6}$$

Following (1), the energy and the length scale depend on the parameter v:

$$\left(1+\frac{Z_1}{Z_2-0.3}\right)^2 = \sqrt{1+2v} \ , \tag{7}$$

or approximately $v \approx 2\,Z_1/Z_2$.

The excitation probability is then given by

$$P = \sum_{n>0} |a_n|^2 \quad . \tag{8}$$

The matrix element $\langle x_{nf}^2\rangle$ is different from zero for

$$\langle x_{nf}^2\rangle = \begin{cases} \frac{1}{2}\sqrt{f(f-1)}, & f = n+2 \\ n+\frac{1}{2}, & n = f \\ \frac{1}{2}\sqrt{n(n-1)}, & n = f+2 \quad . \end{cases} \tag{9}$$

Since the oscillator is initially in the $n = 0$ state, only even states are involved in the excitation process. So the minimum energy transfer for excitation is given by $W_{\min} = 2\hbar\omega_0$. It is now possible to find the relation between the parameter λ (5) and the reduced projectile velocity ξ, since we aim to express the excitation probability as a function of ξ. For atomic collisions, the characteristic time is $\tau = a_K/V$, where V is the incoming projectile velocity. If we adopt the same characteristic time for the excitation process, the parameter λ is related to the reduced projectile velocity $\xi = \hbar V/a_K W_{\min}$ by

$$\lambda = \frac{1}{2\xi} \quad . \tag{10}$$

The probability of a transition into the states $n > 2$ was found to be negligibly small with respect to the probability of a $0 \to 2$ transition. The excitation probability is then well given by $P(0,2)$. In the first-order approximation, this probability is given by

$$P_1(0,2) = \left| -iv\lambda\,\langle x_{02}^2\rangle \int_{-\infty}^{\infty} f(s)\, e^{2i\lambda s}\, ds \right|^2 \tag{11}$$

and in the adiabatic limit by

$$P_2(0,2) = \left| -i \frac{v\lambda}{\sqrt{1+2v}} \langle x_{02}^2 \rangle \int_{-\infty}^{\infty} f(s)\, e^{2i\lambda s\sqrt{1+2v}}\, ds \right|^2 . \tag{12}$$

It is the probability ratio $P_2(0,2)/P(0,2)$ which will be compared to the cross-section ratio of Fig. 1. The calculation of excitation probabilities is considerably simpler than the corresponding problem in atomic mechanics. Due to the strong selection rules (9), the expansion (2) may effectively be terminated for a rather small number of states. Matrix elements are simple analytical expressions and there is no continuum. On the other hand, the time dependence of particular matrix elements is given by a single function f, while in the atom time dependencies of particular matrix elements are different. This requires particular care when choosing f which is at most an approximation of its atomic counterpart.

B. Time dependence of perturbation

In the atom, the most important matrix elements are those coupling the $1s$ state to the continuum and to itself:

$$G = \left\langle k \left| \frac{1}{\mathbf{r} - \mathbf{R}(t)} \right| 1s \right\rangle , \qquad F = \left\langle 1s \left| \frac{1}{\mathbf{r} - \mathbf{R}(t)} \right| 1s \right\rangle . \tag{13}$$

where $\mathbf{r}$ and $\mathbf{R}$ denote the position of the electron and the incoming ion, respectively. The length unit is given by the K-shell radius of the unperturbed atom. The function $f(t/\tau)$ should describe the characteristic time dependencies of F and G. Both functions are time dependent through $\mathbf{R}(t)$ and we shall normalize f, F, and G to unity for $R = 0$. For this reason we shall also omit the usual normalization factors of the wave functions in further derivation. The function F is given by [5]

$$F = \frac{1}{R}\left[1 - (1+R)\, e^{-2R}\right] . \tag{14}$$

For G, we shall assume the monopole approximation, or the contribution of the s partial wave to the continuum:

$$G = \left\langle \Psi_0 \left| \frac{1}{r_>} \right| 1s \right\rangle , \tag{15}$$

where $r_>$ denotes the greater of r and R. The Coulomb function Ψ_0 for $l = 0$ [14] is written for the present purpose as

$$\Psi_0 = \sum_{p=0} \frac{M_p}{(p+1)!}\, r^p . \tag{16}$$

The coefficients M_p are determined by the recursion relation

$$M_p = -\frac{2}{p} M_{p-1} - k^2 M_{p-2} , \qquad M_0 = 1 , \quad M_1 = -2 . \tag{17}$$

Here k^2 is the outgoing electron energy in units of $(Z_2 - 0.3)^2$ Ry; it is related to the transferred energy W by [15]

$$k^2 = W - 1 . \tag{18}$$

After some algebra it may be shown that the following relation holds for M_p:

$$\sum_{p=0}^{\infty} (p+2)\, M_p = 0 \tag{19}$$

while G is given by the expansion

$$G = (1+R)\, e^{-R} + e^{-R} \sum_{p=2}^{\infty} \left(1 + \frac{1}{S(p+1)} \sum_{l=0}^{p-2} (l-p+1)\, M_l \right) \frac{R^p}{p!} ,$$

$$S = \sum_{p=0}^{\infty} M_p . \tag{20}$$

Compared to an earlier expression [16], the series (20) is simpler and numerically stable for quite large values of R. The lowest term is independent of k and it was already used as a low R approximation for the zero-energy matrix element [17]. However, the functions G, F, and $(1 + R)\, e^{-R}$ differ for R^2 and higher terms (Fig. 3).

The expansion (20) is valid for positive and negative values of k^2. For negative values it is possible to expand G in a different way. The final state is virtually bound and its wave function is given by

$$\Psi_0 = e^{-\frac{r}{n}}\, \Gamma\left(1 - n,\, 2,\, \frac{2r}{n}\right) , \tag{21}$$

where n is generally noninteger. Expanding the hypergeometric function into a power series, an expression analogous to (20) is obtained, but with different coefficients M_p, the summation p terminating at the $n - 1$ term for integer n, and with R replaced by $\frac{n+1}{n} R$. Comparison of the lowest term with that of (20) implies that we search

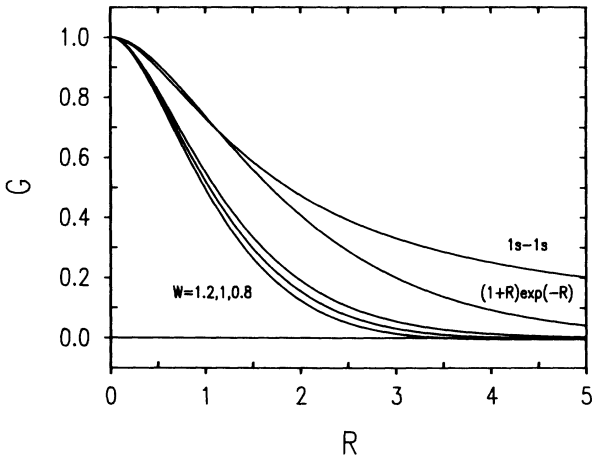

FIG. 3. Radial dependence of the monopole matrix element G for three values of W. Also shown are the $1s - 1s$ matrix element F and the function $(1 + R)\, e^{-R}$. The radial distance is measured in a_K.

the function f in the form

$$f = (1 + \alpha R)\, e^{-\alpha R}, \tag{22}$$

where α is an optional parameter. The choice of f (22) is sensible since for a straight-line trajectory with the impact parameter b, the probability $P_1(0,2)$ is obtained analytically. From [18] we derive a useful formula

$$\int_0^\infty \left(1 + \sqrt{\gamma^2 + x^2}\right) e^{-\sqrt{\gamma^2+x^2}} \cos(\beta x)\, dx$$

$$= \frac{\gamma^2}{1+\beta^2} K_2\left(\gamma\sqrt{1+\beta^2}\right), \tag{23}$$

which yields immediately

$$P_1(0,2)$$

$$= \left| -i \frac{v\,(\alpha\xi)^3 \langle x_{02}^2 \rangle}{1 + (\alpha\xi)^2} (bq_0)^2 K_2\left(bq_0\sqrt{1 + (\alpha\xi)^2}\right) \right|^2 . \tag{24}$$

In the adiabatic limit, $\xi \to 0$, P_1 and the K-shell ionization probability [19] have a rather similar velocity and impact-parameter dependence. Since α then influences P_1 through the α^6 multiplicative factor only, the value of α is not so important for G and can be determined with respect to the function F. Taking $\alpha = 2/\sqrt{3}$, the functions f and F agree up to the R^2 term. It should be noted that higher values of α would move f closer to G; the choice of $\alpha = \frac{3}{2}$ returns an exact expression for G at $W = \frac{3}{4}$.

III. NUMERICAL METHODS

The method of solving (6) was of a modified midpoint type extrapolating the step size to zero [20]. The size of the integration interval was found empirically. The time dependent function f (22) actually depends on the projectile coordinates. The calculation was made for straight-line–constant-velocity projectile trajectories, as well as for hyperbolic trajectories in the Coulomb field. For the latter case, a parametric representation of the hyperbola was used. Since the system of differential equations (6) contains oscillatory functions, we used a somewhat different representation which is linear for large values of the parameter u:

$$s = u + d \ln\left\{ \frac{u}{\epsilon d} + \left[\left(\frac{u}{\epsilon d}\right)^2 + 1 \right]^{1/2} \right\} ,$$

$$R = \sqrt{u^2 + (\epsilon d)^2} + d \ . \tag{25}$$

Here d and ϵ denote half the distance between the projectile and the target nucleus in a head-on collision and the eccentricity of the hyperbola, respectively. The calculations involved states up to $n = 8$, in order to maintain 1% accuracy up to $v = 0.3$.

IV. DISCUSSION

We expected the harmonic-oscillator model to yield reliable results even in its simplest form. For the straight-line projectile trajectories it was found that the ratio P_2/P does not depend strongly on b. So we present results for $b = 0$ and $R = |s|$ (Fig. 4). The value of $\alpha = 2/\sqrt{3}$ was used throughout. The ratio P_2/P of Fig. 4 reproduces a large part of Fig. 1. For faster collisions, $\xi \sim 1$, the adiabatic excitation probability and united-atom cross sections yield too low values. Both quantities become realistic at $\xi \sim 0.6$ but yield too high values for slower collisions. The functions P_2/P and $\sigma_{\mathrm{UA}}/\sigma_{\mathrm{ref}}$ exhibit a broad maximum at $\xi \sim 0.35$. For even slower collisions, the functions behave quite differently.

For very slow collisions, the contribution of p partial waves predominates in the K-shell ionization process on account of the hyperbolic projectile trajectories [3]. It is not possible to find the function f which would correspond both to F and G for dipole transitions. The dipole matrix element G is zero for $R = 0$ and varies as R^{-2} for large R. Since the $1s - 1s$ matrix element remains unchanged, the functions G and F have very different behavior for small R. Nevertheless, it is possible to demonstrate the effect of hyperbolic trajectories in a different way. Dipole transitions shift the mean impact parameter in the atom to much smaller values than predicted by the monopole approximation (Fig. 5). So we calculate the ratio P_2/P for the function f (22) but for $R(t)$ as determined by the hyperbolic trajectory at the atomic mean impact parameter. The results of this calculation are shown in Fig. 6. The high-velocity part of P_2/P is not essentially changed, but there is a strong increase of P_2/P for very low values of ξ.

The structure of the ratio $\sigma_{\mathrm{UA}}/\sigma_{\mathrm{ref}}$ can thus be clearly explained. The maximum at $\xi \sim 0.35$ corresponds to the reduced s-partial-wave cross section and the strong increase at low ξ values to the reduced p-partial-wave cross section. The cross sections are reduced due to the cou-

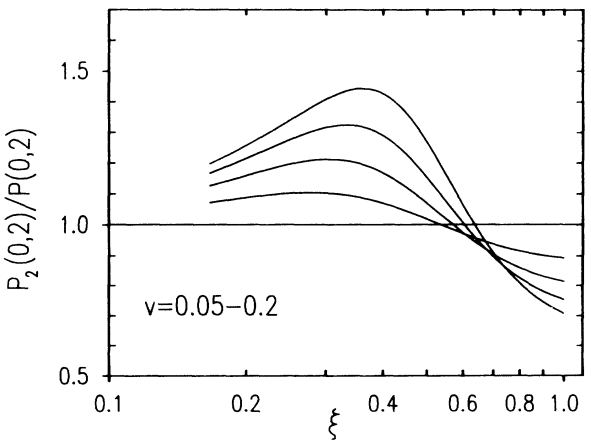

FIG. 4. The ratio P_2/P as a function of the reduced velocity ξ for the straight-line projectile trajectory at zero impact parameter. The values of v are equally spaced from 0.05 to 0.2 and roughly correspond to the ratios Z_1/Z_2 of Fig. 1.

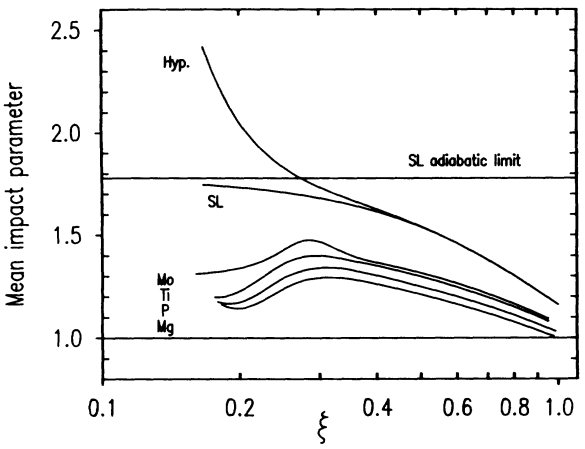

FIG. 5. Mean impact parameter as a function of ξ for protons incident on Mg, P, Ti, and Mo targets. The calculation was performed in the united-atom limit and the results were normalized to q_0^{-1}. SL denotes the mean impact parameter as follows from (24), and Hyp. its value for hyperbolic trajectories.

pling of states. Differences between $\sigma_{\rm UA}/\sigma_{\rm ref}$ and P_2/P for Ti and Mo in Figs. 1 and 6 may be accounted for by relativistic effects which are not included in the oscillator model. Large experimental errors also prevent detailed examination of $\sigma_{\rm UA}/\sigma_{\rm ref}$ in the extreme adiabatic region.

At this point it is also appropriate to discuss the influence of the parameter α (22). Taking $\alpha = 1$ would slightly shift the maxima in Fig. 6 to $\xi \sim 0.4$. Replacing the function f by G from Eq. (20) would shift the maxima down to $\xi \sim 0.25$ since G influences the ground-state wave function much less than the functions F or f.

For other light ions, we examined ^{3}He-Ti and ^{6}Li-Cr collisions (Fig. 7). Experimental data are from [21, 22] and extend down to $\xi \sim 0.3$. The ratio $\sigma_{\rm UA}/\sigma_{\rm ref}$ exhibits a broad maximum at $\xi \sim 0.35$, in accordance with the

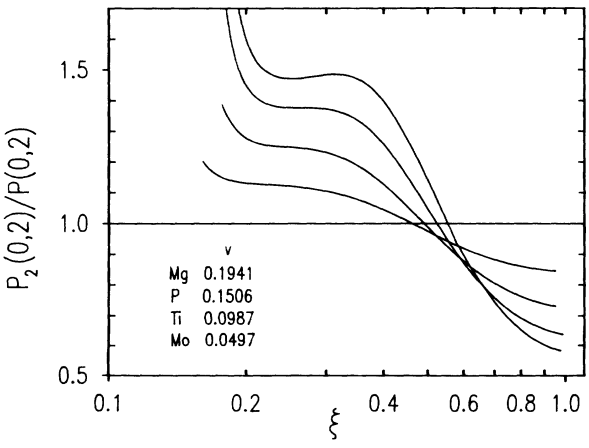

FIG. 6. The ratio P_2/P as a function of ξ for hyperbolic projectile trajectories calculated for the atomic mean impact parameters. Accurate values of v were used.

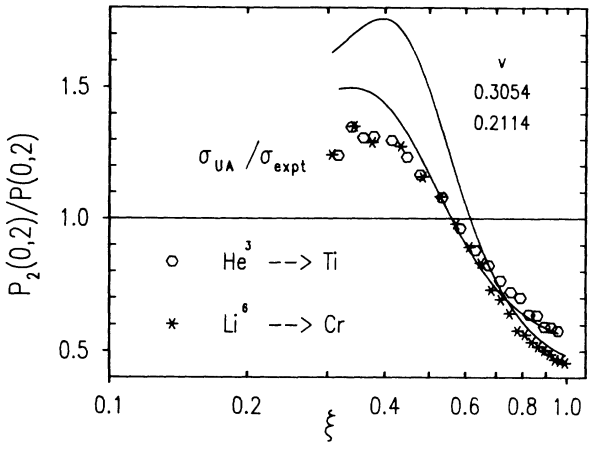

FIG. 7. The ratios P_2/P and $\sigma_{\rm UA}/\sigma_{\rm expt}$ for ^{3}He-Ti and ^{6}Li-Cr collisions, as a function of ξ. Experimental errors are smaller than 8.4% and 13% for Ti and Cr, respectively.

proton data. The maximum is reproduced by P_2/P for ^{3}He-Ti collisions to within 10%. For ^{6}Li-Cr collisions, the position of the maximum is correct, but the values of P_2/P are larger by 30%. Experimental values for ^{3}He-Ti and ^{6}Li-Cr collisions are quite close for $\xi \sim 0.35$, in spite of the different Z_1/Z_2 ratios of 0.09 and 0.125, respectively. Since the height of the maximum is a clear function of Z_1/Z_2 in the case of protons, we can assume that $\sigma_{\rm UA}/\sigma_{\rm ref}$ also depends on Z_1. A possible reason might be the Z_1-dependent increase of the ionization cross section due to parallel ionization processes.

A comparison of Figs. 1 and 6 indicates that for accurate cross-section calculation a coupled-channel approach such as that of [23] is required. As shown by Paul [24], proton cross sections for Cu and Ag [23] agree with the experimental cross sections within 10%. Since calculations of this type [23] are rather complicated, it seems worthwhile to revisit the first-order semiclassical theory and calculate the effective nuclear charge from the harmonic-oscillator model. Numerically, it is possible to find an effective value of $\sqrt{1+2v}$ which renders the results of (12) equal to those of the coupled-channel method. The effective (nonstationary) increase of the nuclear charge is then given by

$$\sqrt{1+2v} = \left(1 + \frac{\Delta Z}{Z_2 - 0.3}\right)^2 . \tag{26}$$

The results of this procedure, based on the values of P according to Figs. 6 and 7, are shown in Fig. 8. The effective increase of the nuclear charge is greater than Z_1 for $\xi \lesssim 0.6$ and attains a nearly universal value of approximately $1.2\,Z_1$ for $\xi \lesssim 0.35$.

The values of ΔZ were used to calculate further effective binding energies. The contribution of the outer-electron screening was calculated from the experimental data in the united-atom approximation. The cross sections, normalized to the experimental values, are shown in Fig. 9. For protons, the structure of Fig. 1 is greatly reduced and the calculated and experimental cross sec-

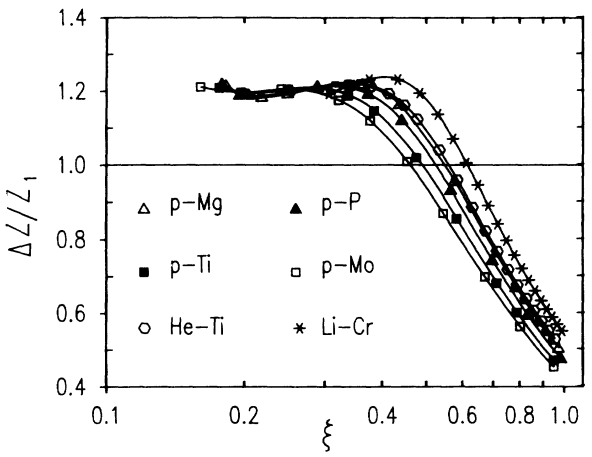

FIG. 8. Effective increase of the nuclear charge as predicted by the harmonic-oscillator model.

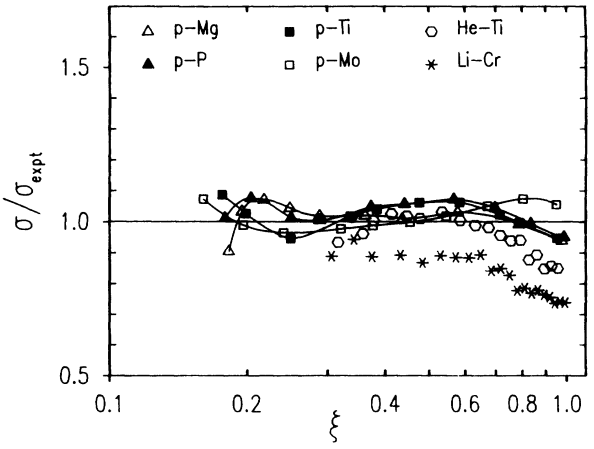

FIG. 9. Semiclassical cross sections, using effective nuclear charges according to Fig. 8 and normalized to the experimental cross sections, as a function of ξ. The lines connecting proton data were obtained by interpolation.

tions agree within 10%. For low values of ξ, the values of $\sigma/\sigma_{\text{expt}}$ are scattered, mostly due to the large experimental errors (see Fig. 1). For $\xi \gtrsim 0.4$, $\sigma/\sigma_{\text{expt}}$ varies with ξ in a way similar to the ratio of the united-atom and Dirac-Hartree-Slater [25] cross sections for Ni and Ag [4]. This suggests that the hydrogenic approximation remains the principal reason for the difference between the semiclassical and experimental cross sections.

There is also good agreement between the calculated and experimental cross sections for ^{3}He-Ti collisions, except for faster collisions $\xi \gtrsim 0.8$. The ratio $\sigma/\sigma_{\text{expt}}$ for ^{6}Li-Cr collisions has a similar ξ dependence though all values are smaller by 15%. Inclusion of $l > 1$ partial waves into the calculation would increase the cross sections and therefore the ratio $\sigma/\sigma_{\text{expt}}$ by several percent for $\xi \sim 1$, but this would not explain the differences in Fig. 9. It seems again that parallel ionization processes are switched for higher Z_1 and ξ values.

Among recent calculations, the cross sections derived using the time-dependent distorted wave functions [12] also reproduced the experimental values rather well. For protons, the cross sections [12] largely overestimated the experimental values for $\xi \lesssim 0.2$. According to the present model, the p-partial-wave contribution to the cross section is strongly reduced as a result of the coupling of states in this velocity region. For ^{3}He-Ti and ^{6}Li-Cr collisions, the present cross sections are slightly closer to the experimental values than those of [12] and would be improved further by extending the calculation to $l > 1$ partial waves.

It is surprising that the harmonic-oscillator model works so well. In a recent study of the ion-atom system [26], the electronic coordinates were transformed into the rotating-coordinate system. In the united-atom limit, the atomic Hamiltonian was indeed that of the perturbed three-dimensional harmonic oscillator.

V. CONCLUSION

At low ion velocities, the coupling of states strongly influences the K-shell ionization cross section. The united-atom limit is not approached in the velocity range accessible to experiments. A model of the harmonic oscillator, where the united-atom limit corresponds to the permanent coupling of the perturbing spring, suggests two regions of the ionization process suppressed below the united-atom limit: one at $\xi \sim 0.35$, responsible for the s partial wave, and the other for $\xi \lesssim 0.2$. The latter region involves a p-partial-wave contribution and results from Coulomb repulsion of the projectile in the field of the target nucleus.

First-order models using hydrogenic wave functions with the effective charges reproduce the proton cross sections within 10%. The present model predicts effective charges which are greater than the corresponding united-atom limit in the velocity range $\xi \lesssim 0.6$.

[1] T. Mukoyama, Int. J. PIXE **1**, 209 (1991).
[2] D. Trautmann and F. Rösel, Nucl. Instrum. Methods **169**, 259 (1980).
[3] J.M. Hansteen, L. Kocbach, and A. Graue, Phys. Scr. **31**, 63 (1985).
[4] Ž. Šmit, Z.Phys. D **22**, 411 (1991).
[5] W. Brandt, R. Laubert, and I. Sellin, Phys. Lett. **21**, 518 (1966).
[6] G. Basbas, W. Brandt, and R. Laubert, Phys. Rev. A **17**, 1655 (1978).
[7] W. Brandt and G. Lapicki, Phys. Rev. A **20**, 465 (1979).
[8] E. Laegsgaard, J.U. Andersen, and M. Lund, in *Proceedings of the Tenth International Conference on Physics of Electron and Atomic Collisions, Paris, 1977*, edited by G. Watel (North-Holland, Amsterdam, 1977).
[9] J.U. Andersen, E. Laegsgaard, and M. Lund, Nucl. In-

strum. Methods **192**, 79 (1982).
[10] O. Benka, M. Geretschläger, and H. Paul, J. Phys. (Paris) Colloq. **12**, C9-251 (1987).
[11] G. Basbas and D.J. Land, Phys. Rev. A **35**, 1003 (1987).
[12] D.J. Land, Phys. Rev. A **44**, 274 (1991).
[13] H. Paul and J. Sacher, At. Data Nucl. Data Tables **42**, 105 (1989).
[14] M. Abramowitz, in *Handbook of Mathematical Functions*, edited by M. Abramowitz and I.A. Stegun (Dover, New York, 1965).
[15] E. Merzbacher and H.W. Lewis, in *Corpuscles and Radiation in Matter II*, edited by S. Flügge, Handbuch der Physik Vol. 34 (Springer-Verlag, Berlin, 1958), p. 166.
[16] M. Pauli and D. Trautmann, J. Phys. B **11**, 667 (1978).
[17] D.J. Land, Nucl. Instrum. Methods, Phys. Res. Sect. B **27**, 491 (1987).
[18] I.S. Gradshteyn and I.M. Ryzhik, *Tablici Integralov, Summ, R'adov i Proizvedenii* (Fizmatgiz, Moscow, 1963), Eq. 3914.
[19] J. Bang and J.M. Hansteen, K. Dan. Vidensk. Selsk. Mat. Fys. Medd. **31**, No. 13 (1959).
[20] W.H. Press, B.P. Flannery, S.A. Teukolsky, and W.T. Vetterling, *Numerical Recipes in C* (Cambridge University, Cambridge, 1988).
[21] D.G. Simons, J.L. Price, D.J. Land, and M.D. Brown, Phys. Rev. A **39**, 3884 (1989).
[22] B. Raith, S. Divoux, and B. Gonsoir, Nucl. Instrum. Methods, Phys. Res. Sect. B **10/11**, 169 (1985).
[23] G. Mehler, W. Greiner, and G. Soff, J.Phys. B **20**, 2787 (1987).
[24] H. Paul, Nucl. Instrum. Methods, Phys. Res. Sect. B **42**, 443 (1989).
[25] M.H. Chen and B. Crasemann, At. Data Nucl. Data Tables **33**, 217 (1985); **41**, 257 (1989).
[26] T.P. Grozdanov and E.A. Solov'ev, Phys. Rev. A **44**, 5605 (1991).